

<https://doi.org/10.1038/s42003-025-09058-9>

# Contact stiffness governs cell mechanosensing through molecular clutches

Check for updates

Peng Zhao<sup>1,5</sup>, Zhaoyi Zhang<sup>2,5</sup>, Ruihao Xue<sup>3,5</sup>, Yang Zheng<sup>2</sup>, Yina Gao<sup>2</sup>, Jialing Cao<sup>1</sup>, Mingwei Jiang<sup>2</sup>, Yuxuan Jiang<sup>2</sup>, Yan Zha<sup>1</sup>, Li Gao<sup>4</sup>, Ze Gong<sup>3</sup>✉, Jing Du<sup>1</sup>✉ & Yanping Cao<sup>2</sup>✉

In cell-extracellular matrix (ECM) interactions, cells apply traction forces to the local ECM through adhesions, in which the local ECM deformation depends on both local and non-local adhesions. Here, we established a nonlocal model based on a contact mechanics-derived parameter—contact stiffness (CS)—to quantify cell-ECM reciprocity. The CS defines the relationship between the local ECM deformation and the total force applied by a cell, integrating the effects of ECM elastic modulus, thickness, cell spreading area, *etc.* We found that both Yes-associated Protein (YAP) activity and the extent of differentiation in human mesenchymal stem cells scaled with CS in power law relation. To investigate the mechanism underlying the mechanosensing by cells, we proposed a CS-based motor clutch model; The excellent agreement between our model predictions and experimental results suggests that various physical or chemical stimuli affects the forces from the molecular clutches by altering the CS. The CS-based motor clutch model elucidates the contributions of time-dependent cell architecture evolution to stem cell differentiation and the influence of a non-adjacent ECM layer on cell behaviours. These results demonstrate that the CS provides a predictive perspective that allows researchers to address longstanding questions about the effects of cell-ECM interactions on cell behaviours.

When cells interact with the extracellular matrix (ECM), they are able to apply physical forces to remodel the surrounding microenvironments, while they can also actively modify their behaviors in respond to the alteration in ECM mechanics<sup>1–3</sup>. Emerging evidence shows that mechanical variables in the cell-ECM system, including ECM elastic modulus<sup>4–6</sup>, ECM thickness<sup>7–9</sup>, and cell spreading area<sup>10,11</sup>, have profound effects on cell behaviors (e.g., motility<sup>12–14</sup>, proliferation<sup>15</sup>, apoptosis<sup>16</sup>, and differentiation<sup>6,17,18</sup>) that are required for processes such as embryonic development<sup>13</sup>, tissue regeneration<sup>19</sup>, and tumor metastasis<sup>20,21</sup>. For example, mesoderm stiffening is essential to triggering neural crest cell migration in *Xenopus laevis*<sup>13</sup>, and stiff matrix promotes tumor metastasis by driving the epithelial-mesenchymal transition of breast tumor cells<sup>5</sup>.

Cells sense and response to mechanical stimuli arising from ECMs through cycles of mechanosensing, mechanotransduction, and

mechanoresponse<sup>2</sup>. The mechanisms underlying cell mechanosensing have been well-explained with motor clutch framework, suggesting that cells perceive alterations in ECM mechanics through the molecular clutches; the kinetics of molecular clutches is governed by an intricate balance between intracellular forces, generated by stress fibers on focal adhesion (FA) plaques, and extracellular traction in the ECM<sup>22–24</sup>. Importantly, previous models mainly discussed the cell mechanosensing of elastic modulus of ECM, which assumed that the local reaction force of the ECM on the cell depends on the local ECM deformation state and ECM modulus. However, contact mechanics theory<sup>25</sup> has established that local ECM deformation depends on both local forces (exerted by local FAs) and non-local forces (imposed by the cell through non-local FAs); i.e., variations in local ECM deformation are induced by changes in the total force, rather than the local force, imposed by the cell on the ECM.

<sup>1</sup>Key Laboratory of Biomechanics and Mechanobiology (Beihang University), Ministry of Education, Beijing Advanced Innovation Center for Biomedical Engineering, School of Biological Science and Medical Engineering, Beihang University, Beijing, China. <sup>2</sup>Institute of Biomechanics and Medical Engineering, AML, Department of Engineering Mechanics, Tsinghua University, Beijing, China. <sup>3</sup>CAS Key Laboratory of Mechanical Behavior and Design of Materials, Department of Modern Mechanics, University of Science and Technology of China, Hefei, Anhui, China. <sup>4</sup>College of Life Science, Hebei Normal University, Hebei, People's Republic of China. <sup>5</sup>These authors contributed equally: Peng Zhao, Zhaoyi Zhang, Ruihao Xue. ✉e-mail: [gongze@ustc.edu.cn](mailto:gongze@ustc.edu.cn); [dujing@buaa.edu.cn](mailto:dujing@buaa.edu.cn); [caoyanping@tsinghua.edu.cn](mailto:caoyanping@tsinghua.edu.cn)

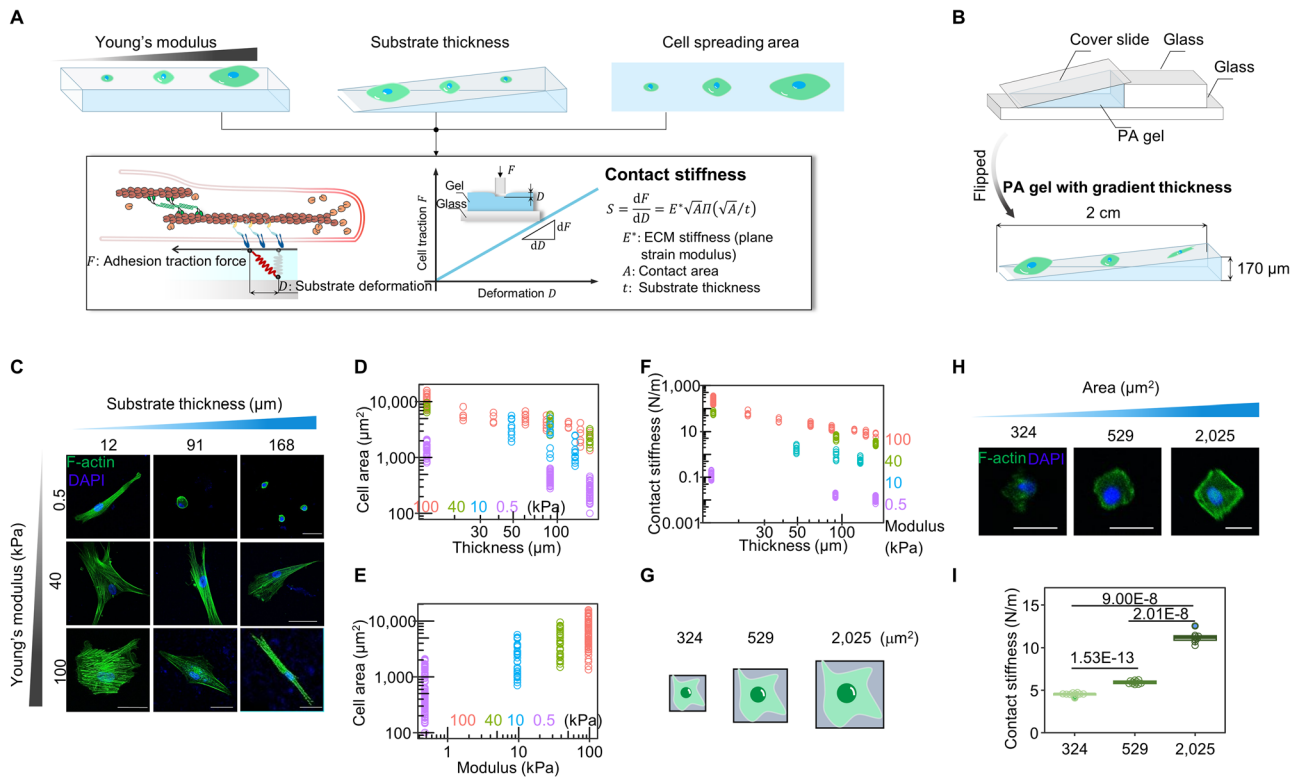


**Fig. 1 | Contact stiffness defines the relationship between local ECM deformation and the force imposed by the cell adhesion.** **A** Schematic diagram of a CS-based frame of reference for interpreting the effects of various ECM mechanics on cell behaviors. CS defines the relationship between local ECM deformation and the force imposed by the cell, integrating mechanical variables such as ECM modulus, ECM thickness, and cell spreading area into one variable. **B** Schematic diagram of the fabrication of ECM composed with a gradient thickness gel. **C** Fluorescence images of hMSCs cultured on gradient thickness gels with moduli of 0.5 kPa, 40 kPa, and 100 kPa were obtained. F-actin and nuclei were stained with phalloidin (green) and DAPI (blue), respectively. Scale bar: 75 μm. **D** Statistical analysis of the cell spreading area of hMSCs cultured on gradient-thickness gels with

moduli of 0.5, 10, 40, and 100 kPa as a function of gel thickness. **E** Statistical analysis of cell spreading area of hMSCs cultured on gradient-thickness gels versus gel modulus. **F** Statistical analysis of contact stiffness in hMSCs cultured on gradient-thickness gels with moduli of 0.5, 10, 40, and 100 kPa across distinct thickness regions. **G** Grey patterns show the relative size of micropatterned fibronectin islands on which cells were grown. **H** Fluorescence images of F-actin and nuclei in hMSCs grown on micropatterned fibronectin islands. F-actin and nuclei were stained with phalloidin (green) and DAPI (blue), respectively. Scale bar: 30 μm. **I** The statistical analysis of contact stiffness in hMSCs grown on a micropatterned fibronectin islands as shown in (H). All error bars are S.E.M. (324 μm<sup>2</sup>: n = 11 cells; 529 μm<sup>2</sup>: n = 12 cells; 2025 μm<sup>2</sup>: n = 8 cells. \*\*\* *P* < 0.001; ns, not significant).

During cell-ECM interactions, the deformation-force relationship depends simultaneously on several ECM-associated variables (including ECM modulus and thickness) and variables related to cell-ECM contact geometry (including cell spreading area and shape). Previous studies focusing on these variables individually have advanced our understanding of how ECM mechanosensing and associated cellular processes regulate diverse physiological and pathological processes<sup>4-11</sup>. However, contact mechanics theory indicates that the effects of these variables are not mutually independent<sup>25</sup>, but rather are coupled in the mechanosensing process<sup>26</sup>. The underlying mechanisms by which these different variables synergistically regulate cell behaviors remain unknown.

To address this issue, we here investigated the contact stiffness (CS), which describes the relationship between local ECM deformation and the cell contractility, in the context of the mechanical effects of the ECM on cell behaviors. Based on contact mechanics theory<sup>25</sup>, CS integrates the effects of different individual parameters (including ECM elastic modulus, ECM thickness, cell spreading area, and cell shape) into one variable that impacts cell-ECM interactions. We assessed ECM mechanosensing in human mesenchymal stem cells (hMSCs) with varying CS values by controlling ECM elastic modulus, ECM thickness, or cell spreading area. The results demonstrated that CS outperformed other individual mechanical variables (*i.e.*, ECM elastic modulus, ECM thickness, and cell spreading area) in characterizing mechanoregulation of YAP activation and stem cell differentiation in both confined and unconfined cell spreading area conditions. Using the concept of CS, we develop a cross-scale model based on the

classical motor clutch model, which reveals the contributions of cell architecture to stem cell differentiation and predicts cellular mechanosensing of a non-adjacent ECM layer. Our findings demonstrate that CS can provide a unified frame for understanding the mechanosensing processes by which cells respond to various mechanical stimuli from ECMs.

## Results

### Contact stiffness defines the relationship between local ECM deformation and the force imposed by a cell

As cells constantly contract and initiates the ECM deformation, the local ECM deformation depends on both the local FA as well as the nonlocal FAs. According to the contact mechanics theory<sup>25,27,28</sup>, the variation in local ECM deformation (*D*) is related to changes in the total force (*F*) from the cell, with their relation determined by the contact stiffness (CS) of ECM. For simplicity, we here proposed to use the CS, derived from a flat punch indenter in contact with ECM half-plane, to understand the cell-ECM interaction (Fig. 1A and Supplementary Fig. S1). Specifically, CS is a variable that integrates the mechanical parameters of the ECM, including ECM modulus, ECM thickness *t*, and the geometric variables defining cell-ECM contact geometry, including the cell spreading area (contact area *A*) and its shape. When the ECM thickness is on the same order as the dimensions of the cell, CS can be expressed as  $S = E^* \sqrt{A} \Pi(\sqrt{A}/t)$ . Here,  $\Pi$  is a dimensionless function and *t* is the ECM thickness<sup>29</sup>. In cases where the ECM is far thicker than a cell (>10-fold), CS can be expressed as  $S = C_0 E^* \sqrt{A}$ , where *C*<sub>0</sub> is a constant; *E*<sup>\*</sup> is the plane-strain modulus (which defines ECM stiffness here)<sup>30</sup>.

Because the CS of the ECM defines the relationship between local ECM deformation and the cell-ECM interaction force and integrates individual variables such as ECM modulus, ECM thickness, cell spreading area and shape<sup>31</sup> into one variable, we examined the use of CS to investigate ECM mechanosensing in a wide range of conditions. To avoid the influence of chemical factors in preparing ECMs with a wide range of CS values, we cultured mechanosensitive hMSCs on a layered ECM composed of polyacrylamide (PA) gel in a gradient of thicknesses on a glass slip (here referred to as a gradient thickness gel) (Fig. 1B and Supplementary Fig. S2). Although the gel elastic modulus was consistent across the gradient, the cell spreading area increased as the gel thickness decreased. The cell spreading area increased from 100 to 15,000  $\mu\text{m}^2$  as the gel thickness decreased from 170 to 12  $\mu\text{m}$  on a 100-kPa gel (Fig. 1C, D). In this system, CS varied as a function of gel thickness. Specifically, CS increased from 5 to 400 N/m as the gel thickness decreased from 170 to 12  $\mu\text{m}$  on a 100-kPa gel (Fig. 1F).

To achieve a wider range of variation in CS, we combined datasets from gradient thickness gels with different moduli (namely 0.5, 10, 40, and 100 kPa), which are composed of ECM modulus, and thickness as well as contact stiffness (Fig. 1C–F). In the combined dataset, the CS ranged over five orders of magnitude from 0.01 to 400 N/m, which was much larger than the range of variation in ECM modulus (Fig. 1C–F). This broad range of CS variations and its physical meaning indicated that CS is more informative in this context than individual variables.

In addition to varying ECM modulus or thickness, we also controlled the cell spreading area by confining cells to the micropatterned islands with different cell spreading areas on the PDMS with the same thickness and stiffness (Fig. 1G). Consistently, the CS increased with the cell spreading area (Fig. 1G, I). Collectively, previous studies of cell-ECM interactions in which individual variables (such as ECM elastic modulus, ECM thickness, or cell spreading area) were tuned also modulated the CS experienced by a cell. Contact stiffness therefore represents a possible promising mechanical variable for interpreting the integrated effects of these individual variables on ECM mechanosensing.

### Contact stiffness outperforms other individual variables of cell-ECM systems in interpreting the mechanoregulation of YAP

Emerging evidence has revealed that YAP activity is regulated by various mechanical variables such as ECM elastic modulus, ECM thickness, and cell spreading area<sup>9,25,32–34</sup>. To reveal the coupled effects of these individual variables, we explored the use of CS for interpreting mechanoregulation of YAP activation. We calculated YAP nuclear translocation in terms of the nuclear/cytoplasmic distribution (N/C ratio) in hMSCs cultured on gradient thickness gels. Immunofluorescence staining showed that the YAP N/C ratio continuously increased along with increases in CS as the ECM modulus remained constant as 100 kPa (Fig. 2A, B). Similar results were observed in hMSCs cultured on gradient thickness gels with different elastic moduli (Fig. 2C, D). These results demonstrate that cells sensed CS rather than ECM modulus when activating YAP.

YAP mechanotransduction is dynamically coupled to actomyosin contractility through RhoA/ROCK-mediated cytoskeletal remodeling<sup>9</sup>. Thus, we further evaluated the use of CS for explaining alterations in YAP activity among cells treated with Cytochalasin, a specific inhibitor of actin polymerization<sup>35</sup>. There was a dose-dependent decrease in CS and a simultaneous decrease in the YAP N/C ratio among Cytochalasin-treated cells (Fig. 2E–G). Notably, the ECM elastic modulus and thickness were maintained at 100 kPa and  $\sim 170 \mu\text{m}$ , respectively, for both treated and untreated cells. We therefore inferred that the observed variations in YAP activity resulted from differences in the CS per se rather than from differences in ECM elastic modulus or thickness (Fig. 2H).

We next combined the experimental datasets described above, analyzing data from cells grown on gradient thickness gels with different elastic moduli and data from cells treated with Cytochalasin. Using the combined dataset, we analyzed the fit between the CS and the YAP N/C ratio. In the form of a power function, CS scaled better with the YAP N/C ratio (with an exponent of  $0.42 \pm 0.012$ ,  $r^2 = 0.826$ ,  $P < 0.001$ ) than other variables did,

including ECM modulus ( $r^2 = 0.063$ ,  $P < 0.001$ ), ECM thickness ( $r^2 = 0.544$ ,  $P < 0.001$ ), and cell spreading area ( $r^2 = 0.623$ ,  $P < 0.001$ ) (Fig. 2I).

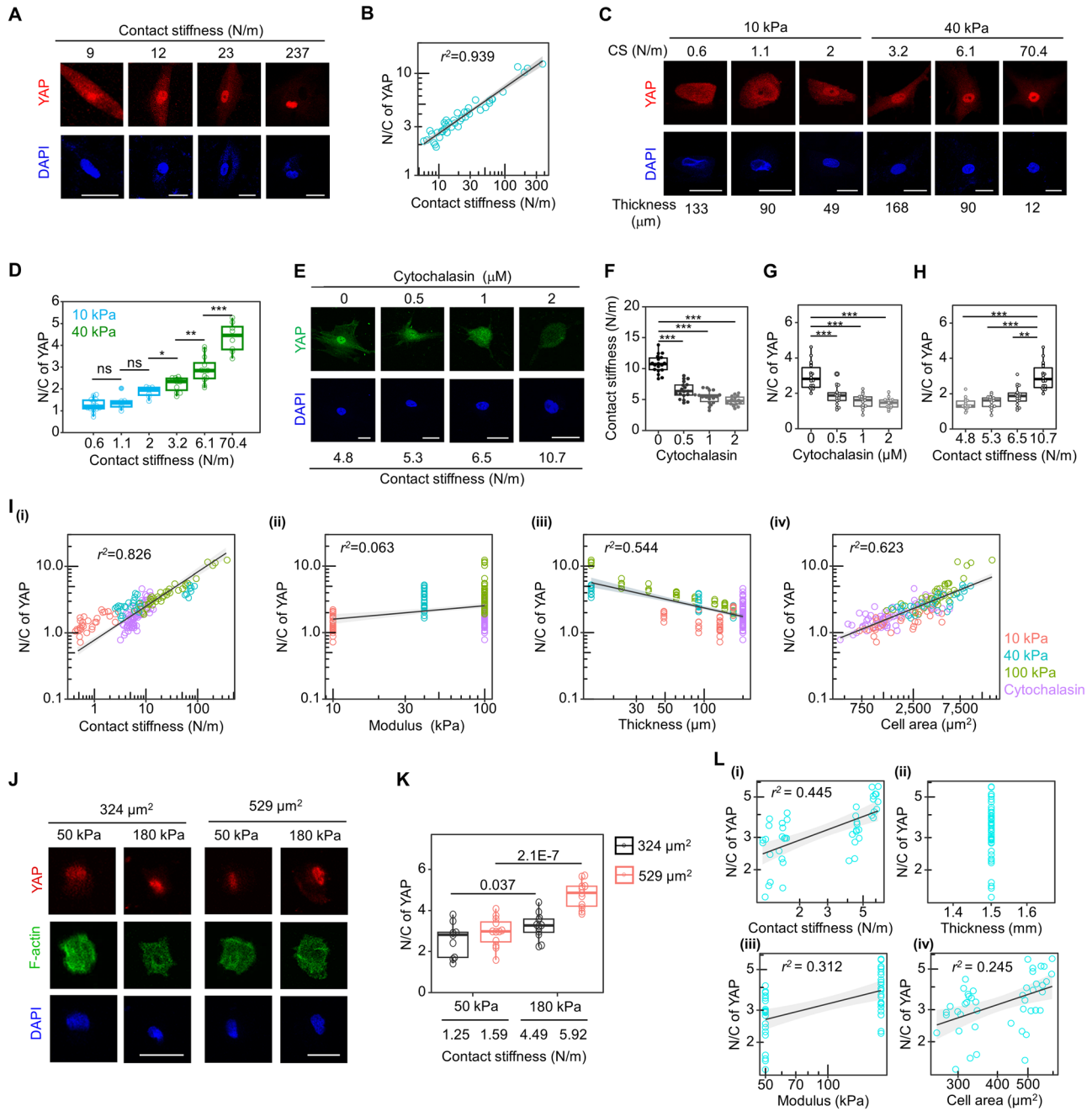
In contrast to in vitro cultured cells on 2D ECM, where spreading is unrestricted, cells in vivo are often mechanically confined by surrounding tissues<sup>36</sup>. To investigate whether contact stiffness interprets the mechanoregulation of cells under spatially constrained conditions, we cultured hMSCs on micropatterned islands with fixed spreading area (324  $\mu\text{m}^2$ ) but varying ECM elastic moduli (50 kPa or 180 kPa). Immunofluorescence staining revealed that, although the cell spreading area was consistent, YAP N/C value was still significantly higher in cells grown on 180 kPa ECM (CS  $\sim 4.49$  N/m) compared with cells grown on 50 kPa ECM (CS  $\sim 1.25$  N/m). Similar results were observed in cells confined to 529  $\mu\text{m}^2$  micropatterned islands (Fig. 2J, K). Using the above dataset, we analyzed the fit between CS and YAP N/C ratio. Consistently, CS scaled better with the YAP N/C ratio ( $r^2 = 0.445$ ,  $P < 0.001$ ) than other variables did, including ECM modulus ( $r^2 = 0.312$ ,  $P < 0.001$ ), and cell spreading area ( $r^2 = 0.245$ ,  $P < 0.001$ ) (Fig. 2L). These results further demonstrate that CS successfully explains YAP mechanosensing in spatially constrained cells.

In addition to the experiments performed in the present study, we also applied CS to interpret YAP mechanosensing in datasets from the literature<sup>10,37,38</sup>. Using published datasets, we found that CS varied significantly between cell types (Supplementary Fig. S3A). However, the YAP N/C ratio consistently scaled well with CS in each cell type (Supplementary Fig. S3B, C). Taken together, these results demonstrate that CS exhibits general superiority in interpreting YAP activation compared with other individual variables in various cell-ECM systems, because CS integrates the effects of different key variables on cell-ECM interactions.

### Contact stiffness-based motor clutch model explains cell spreading and adhesion formation in response to different ECM thicknesses and moduli

Previous studies have demonstrated that cell architecture (e.g., cell spreading area and shape) is regulated by the activity of adhesion molecules (e.g., FA plaques), myosin contractility, and cytoskeleton (e.g., F-actin)<sup>39,40</sup>, of which the mechanism has been explained by the molecular motor clutch framework<sup>24,40–43</sup>. In the previous sections, we have applied the CS to integrate different ECM properties (i.e., modulus, thickness, and cell spreading area) and analyzed its correlation with YAP activation. To further understand how cells can probe the CS and modify their behaviors, we next proposed a CS-based motor clutch model by incorporating the CS into the motor clutch framework (Fig. 3A and Supplementary Fig. S4A). Specifically, we have replaced the local stiffness of the substrate spring with the contact stiffness  $S = E^* \sqrt{AII} (\sqrt{A}/t)$  as stated previously, where we adopted the total adhesion area (i.e., summation of individual FA areas) as the contact area A. Note that, using this corrected contact stiffness S (that adopted adhesion area, instead of cell spreading area, as contact area) doesn't change the trend of model predictions, as our experiments shows that the adhesion area is linearly related to the cell spreading area (Supplementary Fig. S4B). Meanwhile, we considered the cell membrane tension induced by actin polymerization at the leading edge in our model, which is balanced with myosin contractility and FA traction force on the F-actin. During the cell spreading process, the contact area and CS increase, elevating FA traction forces and promoting cell spreading, and the variation in cell spreading also changes the CS in turn, ultimately affecting the relationship between the local ECM deformation and intracellular forces. Consequently, a cross-scale mechanotransduction regulatory loop between intracellular force balances and CS sensing is established.

Using our CS-based motor clutch model (refer to Supplementary Figs. S4 and S5 and Supplementary Note 1), we demonstrate that a larger CS increases the cell spreading as well as the FA area (Fig. 3C, D, black lines). To verify our CS-based motor clutch model, we experimentally assessed how CS affects the assemblies of FA plaques and cell spreading. Using immunofluorescence staining in hMSCs cultured on gradient thickness gels with a constant modulus of 40 kPa, we quantified the FA size and cell spreading area in response to different gel thicknesses (Fig. 3B). Consistent with our



YAP activation results, keeping the same modulus while varying the gel thickness (from 10  $\mu\text{m}$  to 170  $\mu\text{m}$ ) significantly affected single FA and cell spreading areas (rings in Fig. 3C, D); this indicates that cells can sense the gel thickness in addition to the modulus. Meanwhile, our model shows that a thinner ECM elevates the corrected CS, leading to larger FA plaques as well as larger cell spreading areas. Importantly, we found a good agreement between the experimental data and our model predictions in both the FA and cell spreading areas (Fig. 3B–D), which strongly supports the concept of the CS sensed by cells.

As a large ECM elastic modulus also raises CS, we further test our model predictions on how substrate modulus regulates cell architecture (Fig. 3E, F and Supplementary Fig. S5). Our model shows that, when varying the modulus by 3 orders from 0.1 kPa to 100 kPa, the predicted corrected CS changed by 5 orders of magnitude (from  $10^{-1}$  pN/nm to  $10^4$  pN/nm; see Fig. 3E) with the additional 2 orders of magnitude from the contact radius change (from  $10^0$   $\mu\text{m}$  to  $10^1$   $\mu\text{m}$ ; see Fig. 3F) and effects from ECM thickness

(from  $10^1$   $\mu\text{m}$  to  $10^2$   $\mu\text{m}$ ); this magnitude difference aligns with our experimental observation (Supplementary Fig. S4C–H). More interestingly, by extracting the corrected CS from all the experimental data of three different ECM moduli and varied ECM thickness, we found that these data match excellently with our predicted corrected CS vs. cell spreading area relationship (Fig. 3G and Table S2). Overall, our CS-based motor clutch model integrates ECM modulus, thickness, and cell spreading area into the CS, a single quantity sensed by the cell, which provides a more comprehensive view of cellular mechanosensing.

### Contact stiffness interprets the mechanoregulation of stem cell differentiation

Extensive studies have shown that the mechanical micro-environment regulates stem cell differentiation<sup>4,6,44,45</sup>. Here, we assessed whether CS could be used to interpret mechanical stimulus-induced stem cell differentiation. This was accomplished by analyzing the extent of stem cell differentiation

**Fig. 2 | Contact stiffness outperforms other individual parameters of cell-ECM systems in interpreting the mechanoregulation of YAP.** **A** Representative immunofluorescence images of YAP and nucleus in hMSCs grown on a 100 kPa gradient thickness gel at different contact stiffness stained by YAP antibody (red) and DAPI (blue), respectively. Scale bar: 75  $\mu$ m. **B** The statistical analysis of YAP N/C ratio in hMSCs grown on a 100 kPa gradient thickness gel at different contact stiffness as shown in (A). YAP N/C ratio scales as power functions of contact stiffness, with exponent  $0.456 \pm 0.015$  ( $r^2 = 0.939$ ,  $P < 0.001$ ). Grey area are 95% confidence intervals for the fitted functions. **C** Representative immunofluorescence images of YAP and nucleus in hMSCs grown on a 10 or 40 kPa gradient thickness gel at different contact stiffness stained by YAP antibody (red) and DAPI (blue), respectively, Scale bar: 50  $\mu$ m. **D** The statistical analysis of YAP N/C ratio in hMSCs grown on a 10 or 40 kPa gradient thickness gel at different contact stiffness as shown in (C). All error bars are S.E.M. (n = 15, 6, 7, 11, 12, and 9 cells for CS = 0.6, 1.1, 2, 3.2, 6.1, and 70.4 N/m, respectively). **E** Representative immunofluorescence images of YAP and nucleus in hMSCs grown on a 100 kPa gel with constant thickness (larger than 200  $\mu$ m) in the presence of Cytochalasin at different concentrations stained by YAP antibody (red) and DAPI (blue), respectively. Scale bar: 50  $\mu$ m. **F** The statistical analysis of contact stiffness in hMSCs grown on a 100 kPa gel with different concentrations of Cytochalasin as shown in (E). All error bars are S.E.M. (n = 18, 17, 17, and 14 cells for 0, 0.5, 1, and 2  $\mu$ M, respectively). **G** The statistical analysis of YAP N/C ratio in hMSCs grown on a 100 kPa gel with different concentrations of Cytochalasin as shown in (E). All error bars are S.E.M. (n = 18, 17, 17, and 14 cells for 0,

0.5, 1, and 2  $\mu$ M, respectively). **H** The statistical analysis of YAP N/C ratio in hMSCs grown on a 100 kPa gel with different contact stiffness as shown in (E). All error bars are S.E.M. (n = 14, 17, 17, and 18 cells for CS = 4.8, 5.3, 6.5, and 10.7 N/m, respectively). **I** Relationship between YAP N/C ratio and (i) contact stiffness or other parameters ((ii) ECM stiffness, (iii) ECM thickness and (iv) cell spreading area) in hMSCs grown on grown on gradient thickness gels with different stiffness or treated with Cytochalasin. N/C of YAP scales across all the combined datasets as power functions of contact stiffness, with exponent  $0.42 \pm 0.013$  ( $r^2 = 0.826$ ,  $P < 0.001$ ); cell spreading area, with exponent  $0.837 \pm 0.046$  ( $r^2 = 0.623$ ,  $P < 0.001$ ); thickness, with exponent  $-0.48 \pm 0.029$  ( $r^2 = 0.544$ ,  $P < 0.001$ ); modulus, with exponent  $0.213 \pm 0.076$  ( $r^2 = 0.063$ ,  $P < 0.001$ ). **J** Representative images of F-actin or YAP and nucleus in hMSCs grown on micropatterned fibronectin islands at the same thickness regions for 1 days stained by phalloidin (green) or YAP (red) and DAPI (blue), respectively. Scale bar: 30  $\mu$ m. **K** The statistical analysis of N/C of YAP in hMSCs grown on a micropatterned fibronectin islands as shown in (J). All error bars are S.E.M. (n = 9, 12, 21, and 13 cells for CS = 1.25, 1.58, 4.42 and 5.92 N/m, respectively). **L** YAP level scales as power functions of contact stiffness, with exponent  $0.334 \pm 0.06$  ( $r^2 = 0.445$ ,  $P < 0.001$ ); Modulus, with exponent  $0.277 \pm 0.066$  ( $r^2 = 0.312$ ,  $P < 0.001$ ); cell spreading area, with exponent  $0.625 \pm 0.162$  ( $r^2 = 0.245$ ,  $P < 0.001$ ); Grey area are 95% confidence intervals for the fitted functions. Grey area are 95% confidence intervals for the fitted functions. All box-whisker plots show the medians, maxima, minima, upper quartiles and lower quartiles. \* $P < 0.05$ ; \*\* $P < 0.01$ ; \*\*\* $P < 0.001$ ; ns, not significant.

among hMSCs grown on gradient thickness gels. Levels of the osteogenic differentiation markers RUNX2 and Collagen I significantly increased along with increases in CS (Fig. 4). The positive correlations between CS and levels of osteogenic differentiation markers were more pronounced in regions with a high CS (>10 N/m) than in regions with a low CS (<1 N/m) (Fig. 4, Supplementary Fig. S6). These results demonstrated the sensitivity of stem cell differentiation to variations in CS.

Next, we compared the fitting of different variables in the cell-ECM system with the extent of stem cell differentiation. We found that expression levels of all osteogenic differentiation markers scaled with CS much better compared to other variables such as ECM elastic modulus, ECM thickness, or cell spreading area (Fig. 4B, C). These data demonstrate that CS could be successfully used to interpret mechanoregulation of stem cell differentiation.

We then explored the applicability of CS in interpreting the extent of stem cell differentiation induced by treatment with an osteogenic differentiation medium under consistent ECM parameters (e.g., elastic modulus and thickness). CS varied over time in the presence of the osteogenic differentiation medium during stem cell differentiation (Supplementary Fig. S7A–C). Importantly, RUNX2 N/C ratio increased with the CS following a power-law scaling (Supplementary Fig. S8D–F). ECM elastic modulus and thickness were both maintained at a steady state over time while the CS changed; Differences in the cell spreading area and CS, rather than in ECM modulus or thickness, therefore accounted for stem cell differentiation (Supplementary Fig. S7G). Together, the above results indicate that the concept of CS provides a perspective to reassess what is known about the mechanisms underlying stem cell differentiation.

### The CS concept explains the time-dependent stem cell differentiation induced by various physical and chemical factors

Two remarkable features of stem cell differentiation are long-lasting changes in gene expression and time-dependent evolutions in cellular architecture<sup>46</sup>. However, the mechanism by which cell architecture evolves over time and its contributions to the progress of stem cell differentiation remain unclear. We first compared the cell spreading areas of hMSCs grown on ECMs with different thicknesses at distinct time points. Notably, we found significant increases in cell spreading area over time (Fig. 5A, B), which led to time-dependent increases in CS (Fig. 5C). Similar variations in the cell spreading area and CS over time were also observed among hMSCs grown on gels with consistent ECM mechanics that were treated with osteogenic differentiation medium (Supplementary Fig. S7A–C). These results indicate that the evolution of cell architecture led to a corresponding change in CS over time during stem cell differentiation. By assuming that, cells can upregulate

proteins associated with adhesion formation (i.e., increased clutch number in our model) over time during differentiation, our model predicts that longer culture time can increase the contact area, elevate the CS sensed by cells, and subsequently enlarge their spreading area (Fig. 5E, F). This model prediction is consistent with the experimental results of time-dependent evolutions in cellular architecture (Fig. 5G, H).

Based on our CS-based motor clutch model, the increased CS indicated that cells were subject to a greater traction force and hence larger cell spreading area over time; We believe this can potentially affect the progress of osteogenic differentiation. To evaluate this hypothesis, we analyzed expression levels of osteogenic differentiation markers. Immunofluorescence staining showed that RUNX2 N/C ratio was significantly increased over time among all hMSCs, regardless of ECM thickness. Increases in RUNX2 N/C ratio were greater among cells grown on a thin ECM than on a thick ECM (Fig. 5A, D). Similar results were observed in hMSCs treated with osteogenic differentiation medium under constant ECM mechanics (Supplementary Fig. S7E, F). We then inhibited time-dependent CS increases by culturing hMSCs on micropatterned islands with constrained cell spreading areas (Fig. 5I). Immunofluorescence staining showed a consistent decrease in both CS and RUNX2 levels in the physically-constrained cells (Fig. 5J–L), indicating that the evolution of CS over time is required for stem cell differentiation. In combined datasets, we further found that CS ( $r^2 = 0.66$ ,  $P < 0.001$ ) scaled as well as cell spreading area ( $r^2 = 0.66$ ,  $P < 0.001$ ) with the RUNX2 N/C ratio in the form of power functions and better than other individual variables did (e.g., ECM modulus or thickness, Fig. 5M). These results demonstrate that the time-dependent evolution CS contributes to stem cell differentiation induced by various physical and chemical factors.

### CS-based motor clutch model predicts the effect of a non-adjacent layer of composite ECM on cell behaviours

The ECMs of living organisms are not homogeneous materials. ECMs can form layered composites with hierarchically-structured assemblies of diverse biological materials<sup>13,47</sup>. Depending on the topographical positions, ECMs are generally divided into a pericellular matrix, such as basement membranes (BMs), and an underlying interstitial matrix, such as ECMs in connective tissues. The pericellular matrix is in direct contact with cells and provides an adhesive microenvironment for resident cells (e.g., epithelial cells), whereas the interstitial matrix underlies the pericellular matrix and supports mechanical tissue integrity<sup>43</sup>. Previous studies of mechanical-based cell behavioral regulation by ECMs have focused on the ECM layer located adjacent to the cell (e.g., the pericellular matrix, here referred to as the

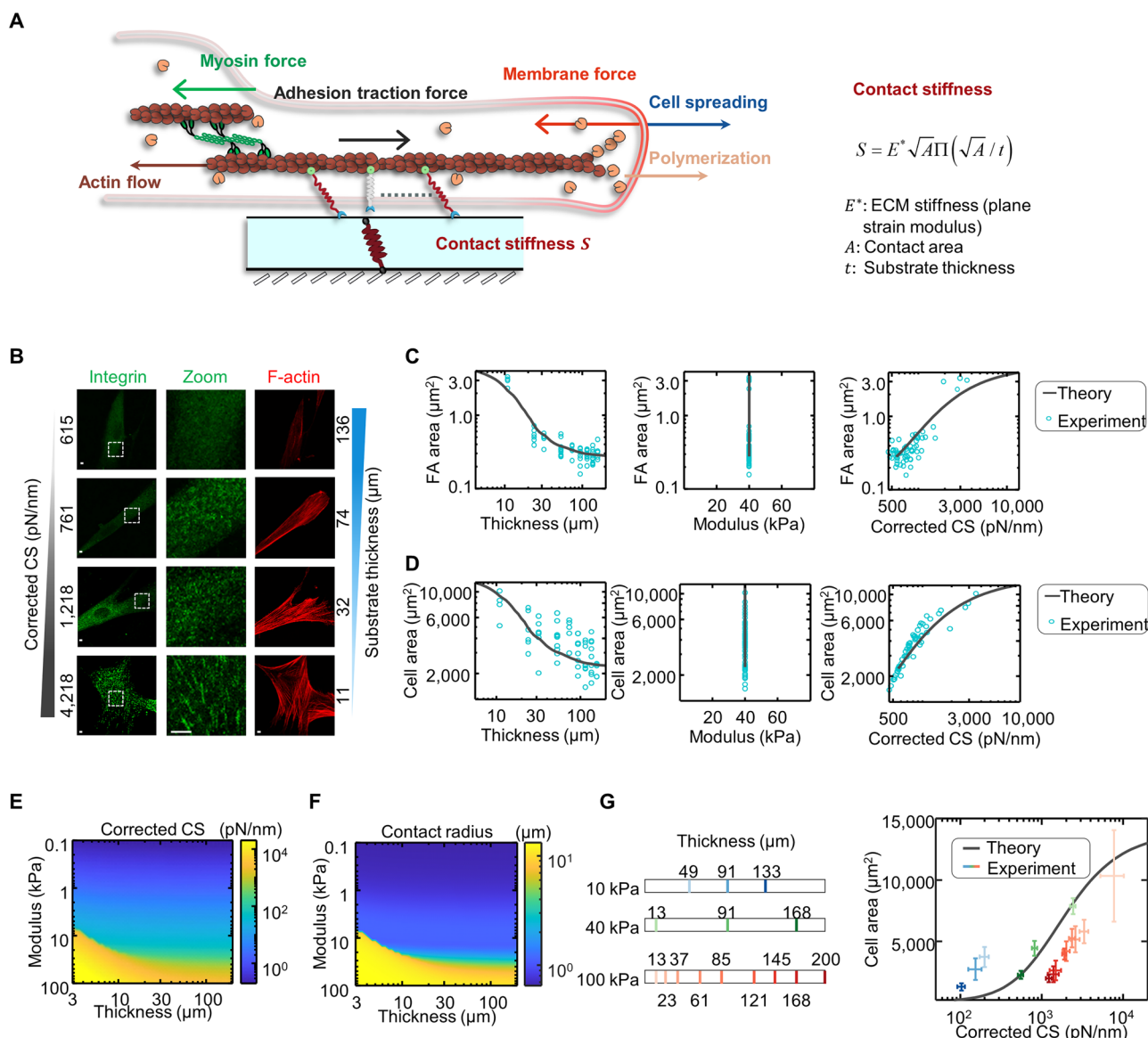


**Fig. 3 | Contact stiffness-based motor clutch model explains cell spreading and adhesion formation in response to different substrate thicknesses and moduli.**

**A** Schematic diagram of the CS-based motor-clutch model. Myosin motors drag the F-actin toward the cell center, generating actin flow. The molecule clutches within this adhesion connect the substrate and the actin bundle, resisting the retrograde flow. Meanwhile, at the cell edge, G-actin polymerizes into F-actin and pushes the cell membrane forward causing cell spreading. The CS sensed by FAs is denoted as  $S$ . **B** Representative images of integrin and F-actin in hMSCs grown on a 40 kPa gradient thickness gel with different contact stiffness and stained by  $\beta 1$  integrin antibody (red) and Phalloidin (green), respectively. The fluorescence images in the middle are enlarged views of the left white dotted boxes. Scale bar: 50  $\mu\text{m}$ . **C, D** The

cell spreading area (**C**) and focal adhesion area (**D**) are plotted with thickness (top panels), elastic modulus (middle panels), and CS (bottom panels). Cyan rings are experimental data, and grey curves are theory predictions. **E, F** Heat maps of CS (**E**) and contact radius (**F**) are plotted as a function of the substrate thickness and elastic modulus. **G** The theoretical cell spreading area aligns with our experimental results in PA gels with different moduli and a thickness gradient. The red, green, and blue color bars refer to substrate thickness with moduli of 100 kPa, 40 kPa, and 10 kPa, respectively. The error bars represent the 95% confidence interval of the experimental data, and the grey curve is our theory prediction. The sample sizes are summarized in Table S2.

adjacent ECM layer). However, from the definition of CS, non-adjacent ECM layers (such as the interstitial matrix) would also affect CS of the composite ECM<sup>28,48</sup>, influencing the reaction force of the ECM on the cell when the ECM was deformed.

To experimentally validate the influence of CS, we prepared a two-layered ECM with a thickness gradient. This consisted of an adjacent ECM layer with a constant modulus of 10 kPa and a non-adjacent ECM layer with either 40 kPa modulus (the 10/40-kPa gel) or 100 kPa modulus (the 10/100-kPa gel) (Fig. 6A). Using this experimental system, we cultured hMSCs and analyzed the responses of cells to variations in non-adjacent ECM layer mechanics. Compared with cells cultured on the 10/

40-kPa gel, cells cultured on the 10/100-kPa gel exhibited larger cell spreading areas at distinct regions of thickness (Fig. 6B, C). By calculating CS based on measurements of individual variables, we found that CS was greater on the 10/100-kPa gel than on the 10/40-kPa gel at distinct thickness regions (Fig. 6D). Importantly, by substituting the CS of the two-layered ECM into our CS-based motor clutch model, our model is able to predict the experimental observations quantitatively (Fig. 6E). To investigate whether cells could sense mechanical stimuli from the non-adjacent ECM layer, we analyzed YAP activity among hMSCs cultured on the two-layered ECMs. Immunofluorescence staining showed that cells cultured on the 10/100-kPa gel had significantly higher YAP N/C

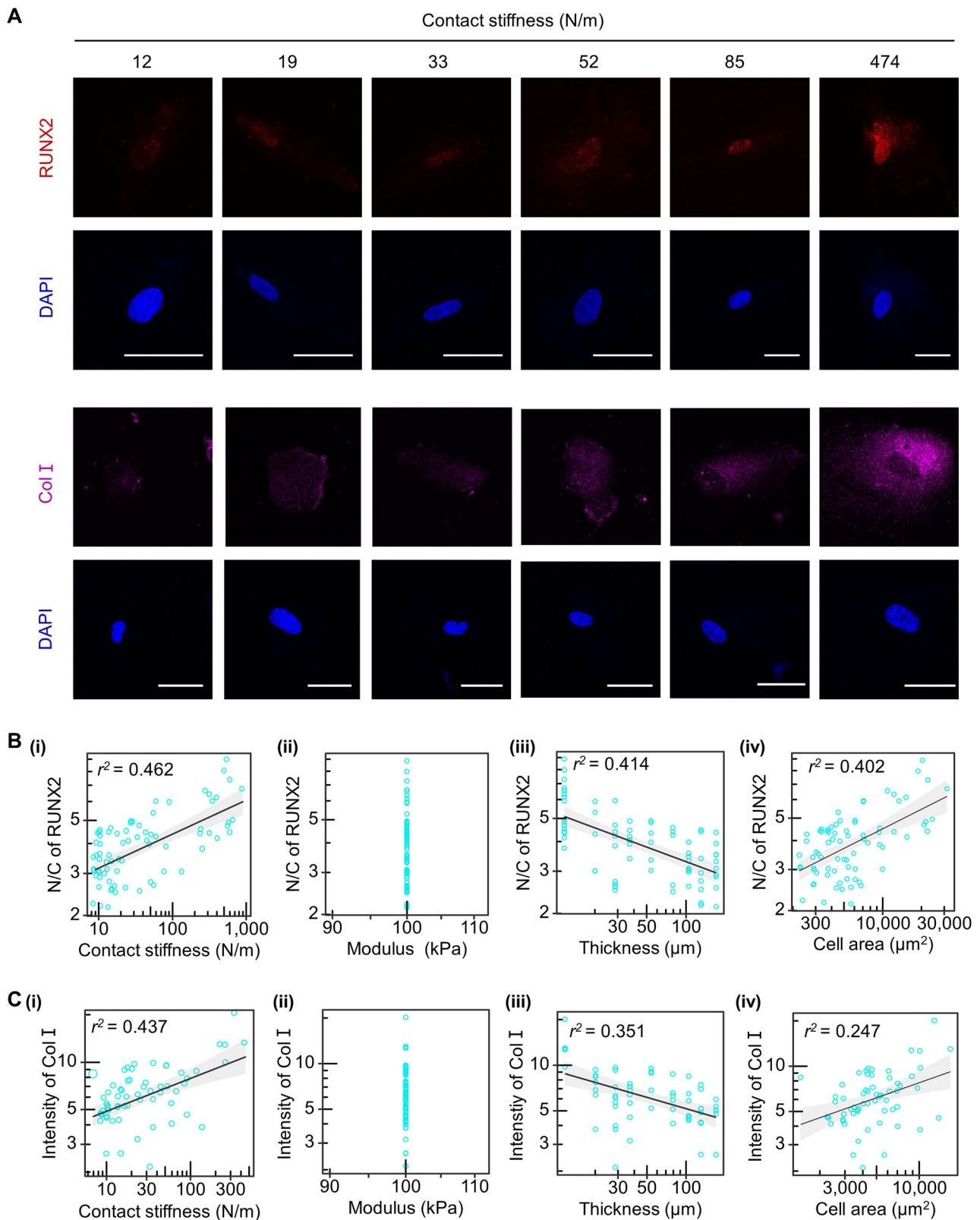
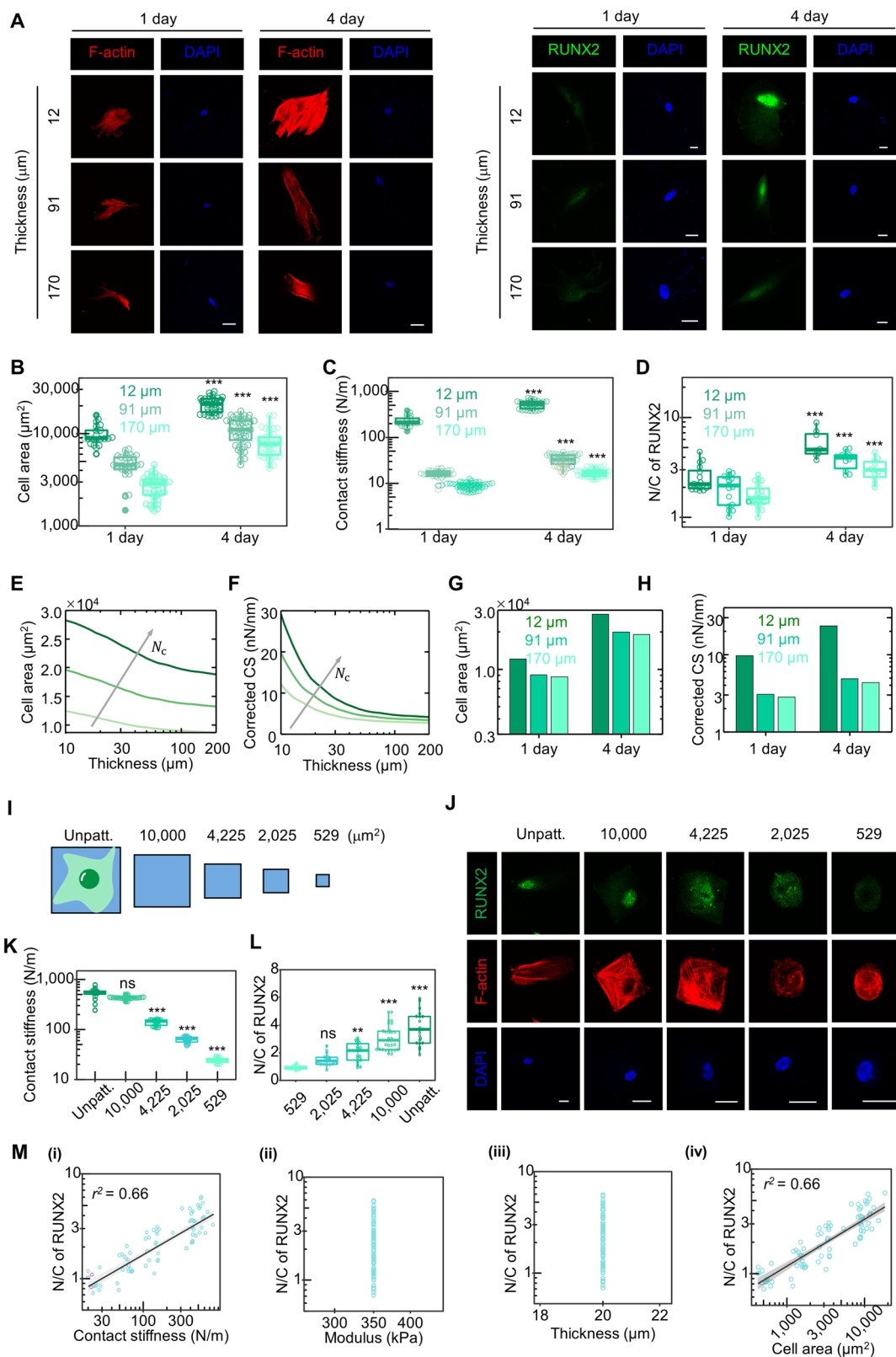


**Fig. 4 | The CS concept interprets the mechanoregulation of stem cell osteogenic differentiation.** **A** Representative immunofluorescence images of RUNX2 and Collagen I (Col I) in hMSCs grown on a 100 kPa gradient thickness gel for 4 days at different contact stiffness stained by RUNX2 (red) or Collagen I antibody (purple) and DAPI (blue), respectively. Scale bar: 50  $\mu\text{m}$ . **B, C** Relationship between **B** RUNX2 and **C** Collagen I level with contact stiffness or other parameters (ECM modulus, ECM thickness and cell spreading area) in hMSCs grown on a 100 kPa gradient thickness gel for 4 days. **B** RUNX2 level scales as power functions of contact

stiffness, with exponent  $0.146 \pm 0.017$  ( $r^2 = 0.462$ ,  $P < 0.001$ ); Thickness, with exponent  $-0.224 \pm 0.031$  ( $r^2 = 0.414$ ,  $P < 0.001$ ); cell spreading area, with exponent  $0.301 \pm 0.039$  ( $r^2 = 0.402$ ,  $P < 0.001$ ); Grey area are 95% confidence intervals for the fitted functions. **C** Col I level scales as power functions of contact stiffness, with exponent  $0.264 \pm 0.034$  ( $r^2 = 0.437$ ,  $P < 0.001$ ). Thickness, with exponent  $-0.278 \pm 0.037$  ( $r^2 = 0.351$ ,  $P < 0.001$ ); cell spreading area, with exponent  $0.467 \pm 0.094$  ( $r^2 = 0.247$ ,  $P < 0.001$ ). Grey area are 95% confidence intervals for the fitted functions.



ratios than cells cultured on the 10/40-kPa gel at distinct thickness regions (Fig. 6F, G). Interestingly, when comparing the datasets from the 10/40-kPa and 10/100-kPa gels at different thicknesses, we found that the YAP N/C ratios were similar only if the CS values were comparable, despite differences in the ECM thickness or non-adjacent layer modulus. For example, the YAP N/C ratios were similar between cells grown on a

10/40-kPa gel that was 45 μm thick (CS = 0.81 N/m) and those grown on a 10/100-kPa gel that was 130 μm thick (CS = 1.04 N/m) (Fig. 6F, G). Moreover, the YAP N/C ratio scaled better with CS than with other individual variables (namely ECM modulus or thickness or cell spreading area) (Fig. 6H). These findings reveal that the regulatory effects of mechanical stimuli from a non-adjacent ECM layer on cells could be

**Fig. 5 | The time-dependent evolution of the CS contributes to stem cell differentiation induced by various physical and chemical factors.** **A** Representative images of F-actin or RUNX2 and nucleus in hMSCs grown on a 100 kPa gradient thickness gel at distinct thickness regions for 1 or 4 days stained by phalloidin (red) or RUNX2 (green) and DAPI (blue), respectively. Scale bar: 50  $\mu\text{m}$ . **B–D** The statistical analysis of cell spreading area (**B**), contact stiffness (**C**), and RUNX2 N/C ratio (**D**) in hMSCs grown on a 100 kPa gradient thickness gel at distinct thickness regions for 1 or 4 days as shown in (**A**). All error bars are S.E.M. **B, C** 1 day:  $n = 21$  cells for 12  $\mu\text{m}$ ;  $n = 28$  cells for 91  $\mu\text{m}$ ;  $n = 42$  cells for 170  $\mu\text{m}$ . 4 day:  $n = 33$  cells for 12  $\mu\text{m}$ ;  $n = 48$  cells for 91  $\mu\text{m}$ ;  $n = 40$  cells for 170  $\mu\text{m}$ . **D** 1 day:  $n = 20$  cells for 12  $\mu\text{m}$ ;  $n = 16$  cells for 91  $\mu\text{m}$ ;  $n = 22$  cells for 170  $\mu\text{m}$ . 4 day:  $n = 8$  cells for 12  $\mu\text{m}$ ;  $n = 10$  cells for 91  $\mu\text{m}$ ;  $n = 11$  cells for 170  $\mu\text{m}$ . \*\*\*  $P < 0.001$ . **E, F** The cell area (**E**) and contact stiffness (**F**) predicted by the CS-based motor model are plotted as a function of substrate thickness. The grey arrows indicate shifts in curves as the clutch number increases. Results were obtained from  $N_c = 1000, 1250, \text{ and } 1500$

interpreted as influencing the reaction force provided by the ECM to the cell due to its contribution to CS.

## Discussion

In cell-ECM interactions, cells are continuously exposed to physical forces imposed by the ECM. Understanding the mechanisms by which such physical forces are generated requires an understanding of the relationship between ECM deformation and the ECM reaction force on a cell<sup>1–3</sup>. The CS of the ECM defines the relationship between the local ECM deformation and the force from the cell (which equals the reaction force of the ECM on a living cell). We therefore proposed a CS-based frame to investigate ECM mechanosensing. Our experiments reveal the advantages of modeling such dynamics with CS rather than individual variables (e.g., ECM elastic modulus, ECM thickness, or cell spreading area) to interpret ECM mechanosensing. The experimental data demonstrated that YAP activation and the extent of stem cell differentiation triggered by tuning these individual variables can ultimately be understood as modulations of CS. Thus, the application of CS concept could provide a neoteric perspective for understanding the common mechanisms underlying the mechanoregulation of multiple ECM stimuli.

Based on the multi-scale features through which cells interact with the ECM, we proposed a CS-based model built on classical motor clutch models; his showed that local ECM deformation is induced by not only the FAs contacting a local position but also the FAs of the entire cell in a long-range, non-local manner. Such a force-deformation relationship can be defined by CS, which integrates the effects of ECM modulus and thickness and the cell spreading area and shape on cell-ECM interactions at the cellular level.

The CS-based motor-clutch model predicted that dynamic variations occurred in parameters from mechanosensitive assembly of single FA plaques to the overall cell architecture, including the cell spreading area and shape over time. All of these factors influenced the CS and therefore ultimately influenced interactions between cells and the ECM. Therefore, our CS-based model can help to explain the dynamic features involved in ECM mechanosensing, mechanotransduction, and mechanoresponse. Our experiments showed that variations in the CS range differed significantly between different types of cells grown on the same gradient thickness gel and hMSCs had the widest CS range of all the cell types analyzed (Supplementary Fig. S8). This indicated that time-dependent architectural reorganization was more active in stem cells than in other differentiated cells in response to mechanical stimuli, which contributed to their differentiation. In the presence of ECM prestress, where the strain energy of the ECM has been suggested as the mechanical variable that is sensed by a cell<sup>49</sup>, the CS can be expressed as  $S = C_0 E^* \sqrt{A} \left[ (1 + \kappa^2)^2 - 4\kappa \right] / (\sqrt{\pi} (\kappa^2 - 1) \kappa^{4/3})$  where  $\kappa \geq 1$  measures the extent of pre-tension<sup>50</sup>. This analytical solution shows that pre-tension increases the CS and leads to a larger cell spreading area, consistent with previous reports<sup>49</sup>.

Taken together, our findings demonstrate that CS is a key mechanical variable that can be sensed and actively tuned by cells. This variable provides

respectively. **G, H** Barplot of the CS-based motor model predicted cell area (**G**) and contact stiffness (**H**) for 1 or 4 days. The results for 1 day and 4 days were obtained for  $N_c = 1000$  and 1500 respectively. **I** Grey patterns show the relative size of micro-patterned fibronectin islands on which cells were grown. Outline of a cell is shown superimposed to the leftmost unpatterned area (Unpatt). **J** Representative images of RUNX2 (green), F-actin (red) and nucleus (blue) in hMSCs grown on micro-patterned fibronectin islands. Scale bar: 50  $\mu\text{m}$ . **K, L** The statistical analysis of contact stiffness (**K**) and RUNX2 N/C ratio (**L**) in hMSCs grown on a micropatterned fibronectin islands as shown in (**J**). All error bars are S.E.M. (Unpatt.:  $n = 16$  cells; 10,000  $\mu\text{m}^2$ ;  $n = 30$  cells; 4225  $\mu\text{m}^2$ ;  $n = 17$  cells; 2025  $\mu\text{m}^2$ ;  $n = 17$  cells; 529  $\mu\text{m}^2$ ;  $n = 12$  cells. \*\*\*  $P < 0.001$ ; *ns*, not significant; compared to Unpatt). **M** RUNX2 N/C ratio scales as power functions of contact stiffness, with exponent  $0.445 \pm 0.042$  ( $r^2 = 0.66$ ,  $P < 0.001$ ); cell spreading area, with exponent  $0.477 \pm 0.046$  ( $r^2 = 0.66$ ,  $P < 0.001$ ); Grey area are 95% confidence intervals for the fitted functions.

a frame of reference for future exploration of cross-scale and dynamic mechanisms of mechanical cell-ECM interactions and the effects of various mechanical stimuli in ECMs. This framework will enable a deeper, more comprehensive understanding of the mechanosensing mechanisms that respond to the ECM as part of many physiological and pathological processes, including embryonic development, tissue regeneration, and tumor metastasis.

## Methods

### Fabrication of PA hydrogels with gradient thickness

Single-layer polyacrylamide (PA) hydrogel molds were constructed using two glass slides (70  $\times$  24  $\times$  1 mm and 24  $\times$  24  $\times$  0.17 mm, CITOTEST® Scientific Co., China) following the assembly scheme in Fig. 1B. For double-layer constructs, a 70  $\times$  24  $\times$  0.17 mm slide and two 24  $\times$  24  $\times$  0.17 mm slides were configured as illustrated in Fig. 6A. PA hydrogels synthesized according to established protocols<sup>51</sup> were prepared through the following steps:

Precursor solutions were injected into the inter-sandwich cavity formed by clamped glass slides separated to establish a triangular cross-section. For layered hydrogels, the second PA layer was sequentially cast onto prefabricated single-layer substrates. Fabricated hydrogels were demolded, transferred to sterile culture dishes (Corning®), and preserved in PBS (pH 7.4) at 4°C until functionalization via sulfosuccinimidyl 1-6- (4'-azido-2'-nitrophenylamino) hexanoate (Sulfo-SANPAH) conjugation as previously described<sup>51</sup>.

Notes: According to the model of PA adhesive preparation, in advance the 24 $\times$ 24 $\times$ 0.17 mm cover slide is adhered to the 74 $\times$ 24 $\times$ 0.17 mm slide. Material preparation to ensure that the hydrogel liquid will not flow into the gap during gel preparation and reduce the thickness variation. Calibrated gauge block + digital caliper ensure that the length of the gel prepared each time is 2 cm. This ensures that the PA hydrogels prepared each time are  $20.00 \pm 0.15$  mm.”

The side profile of the PA and PDMS gel was imaged in bright field using optical coherence tomography (OCT). The obtained images were processed using Image J. The horizontal axis of the gel was divided into ten equal segments, and the thickness at each position was measured. By analyzing the thickness of the PA gel along the X-axis using OCT, a standard curve correlating thickness (Y) with cell position along the X-axis was established. The relationship was determined to be:  $Y = 83.41 X + 7.496$  (Supplementary Fig. S2A, B). Based on the X-position of the cells, the corresponding substrate thickness at the cell location was calculated using this formula.

### Preparation and thickness measurement of PDMS materials

The PDMS used in this paper were Sylgard 527 gel and Sylgard 184 elastomer (Dow Corning), which allows the PDMS substrates were prepared with adjustable mechanical properties<sup>52</sup>. Using an instrument, part A and Part B of Sylgard 527 gel were mixed in a ratio of 1:1 for 2 minutes at 2000 RPM according to the instrument manufacturer's instructions, and then

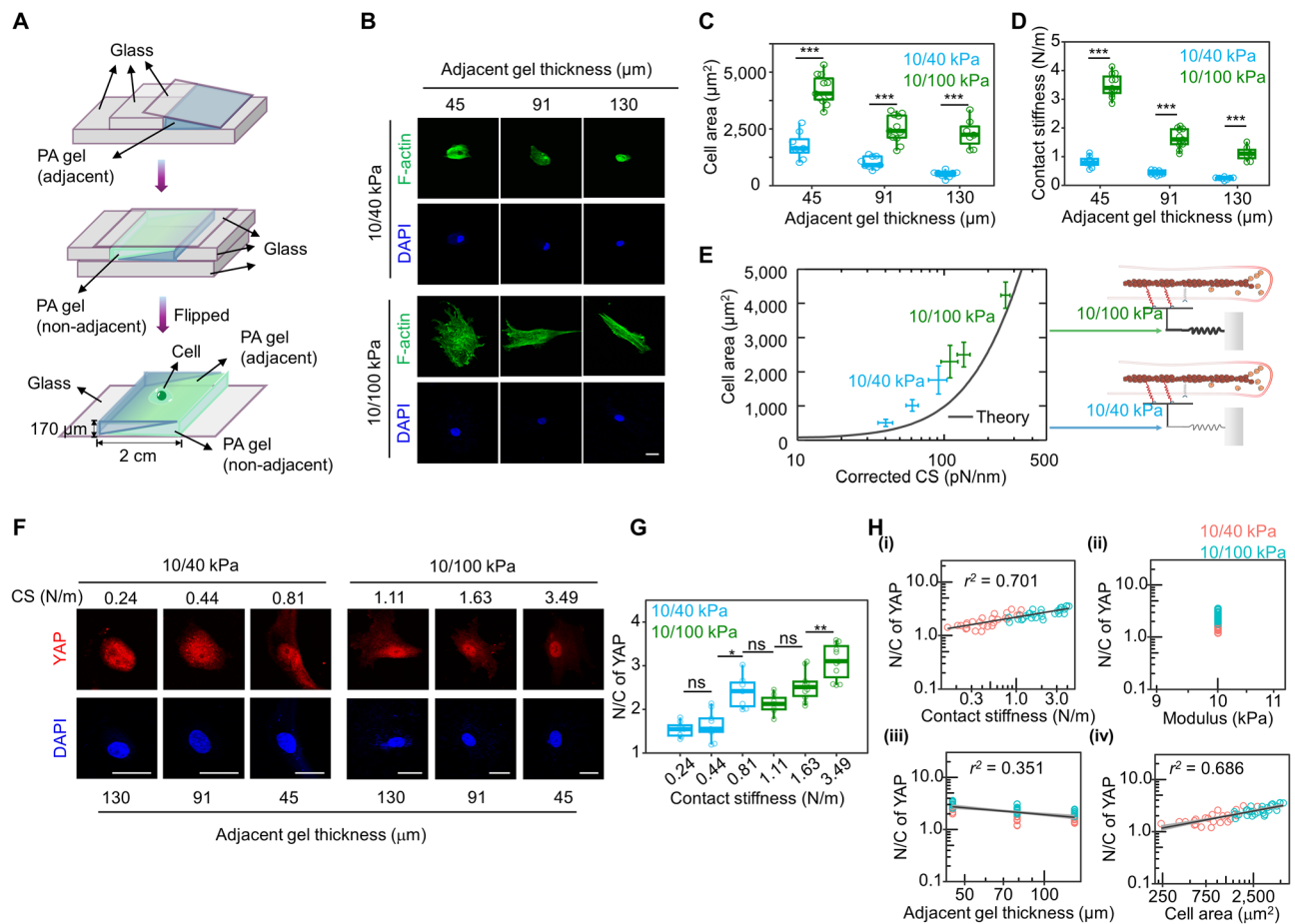


**Fig. 6 | The CS-based motor clutch model predicts the effect of a non-adjacent layer of composite ECM on cellular mechanosensing.** **A** Schematic diagram of the fabrication of a two-layered ECM with gradient thickness composed of a cell adjacent layer and a cell non-adjacent layer. **B** Representative images of F-actin and nucleus in hMSCs grown on two-layered gradient thickness ECMs composed of a cell adjacent layer with constant elastic modulus of 10 kPa and a non-adjacent layer with varied elastic modulus of 40 (10/40 kPa) or 100 kPa (10/100 kPa) gel at distinct thickness regions stained by phalloidin (green) and DAPI (blue), respectively. Scale bar: 30  $\mu\text{m}$ . **C** The statistical analysis of cell spreading area in hMSCs grown on two-layered gradient thickness ECM at distinct thickness regions as shown in (B). All error bars are S.E.M. (n = 8 and 11 cells for 45  $\mu\text{m}$  thickness of 10/40 kPa and 10/100 kPa, respectively; n = 9 and 11 cells for 91  $\mu\text{m}$  thickness of 10/40 kPa and 10/100 kPa, respectively; n = 8 and 7 cells for 130  $\mu\text{m}$  thickness of 10/40 kPa and 10/100 kPa, respectively. \*\*\*  $P < 0.001$ ). **D** The statistical analysis of contact stiffness in hMSCs grown on two-layered gradient thickness ECMs at distinct thickness regions as shown in (B). All error bars are S.E.M. (n = 8 and 11 cells for 45  $\mu\text{m}$  thickness of 10/40 kPa and 10/100 kPa, respectively; n = 9 and 11 cells for 91  $\mu\text{m}$  thickness of 10/40 kPa and 10/100 kPa, respectively; n = 8 and 7 cells for 130  $\mu\text{m}$  thickness of 10/40 kPa and 10/100 kPa, respectively. \*\*\*  $P < 0.001$ ). **E** The model predicted cell area (grey line) and experimental measurement in two-layered PA gels with varying non-

adjacent gel moduli and a thickness gradient in the adjacent gel. The error bars represent the 95% confidence interval of the experimental data, obtained from two-layered ECMs with moduli of 10/100 kPa and 10/40 kPa, respectively. Results were obtained from  $f_{\text{tailin}} = 3\text{pN}$ . **F** Representative immunofluorescence images of YAP and nucleus in hMSCs grown on two-layered gradient thickness ECMs at different contact stiffness stained by YAP antibody (red) and DAPI (blue), respectively. Scale bar: 30  $\mu\text{m}$ . **G** The statistical analysis of YAP N/C ratio in hMSCs grown on two-layered gradient thickness ECMs at different contact stiffness as shown in (E). All error bars are S.E.M. (n = 8, 9, 7, 7, 10, and 11 cells for CS = 0.24, 0.44, 0.81, 1.11, 1.63, and 3.49 N/m, respectively. \*\*\*  $P < 0.001$ ; ns, not significant; compared to Unpatt). \*  $P < 0.05$ ; \*\*  $P < 0.01$ ; \*\*\*  $P < 0.001$ ; ns, not significant). **H** Relationship between YAP N/C ratio and contact stiffness or other parameters (ECM modulus, ECM thickness, and cell spreading area) in hMSCs grown on two-layered gradient thickness ECMs. All box-whisker plots show the medians, maxima, minima, upper quartiles and lower quartiles. N/C of YAP scales across all the datasets as power functions of contact stiffness, with exponent  $0.263 \pm 0.025$  ( $r^2 = 0.701$ ,  $P < 0.001$ ); Thickness, with exponent  $-0.417 \pm 0.065$  ( $r^2 = 0.351$ ,  $P < 0.001$ ); cell spreading area, with exponent  $0.34^2 \pm 0.034$  ( $r^2 = 0.686$ ,  $P < 0.001$ ); Grey area are 95% confidence intervals for the fitted functions.

defrosted at 2000 RPM for 2 minutes. Sylgard 184 elastomer was prepared by mixing 10 parts base to 1 part curing agent using the same mixing and defoaming. According to the ratio method Sylgard 184:527 in the literature getting 50 and 180 kPa PDMS materials that were prepared with two different mass ratios of 1:10 and 1:5. After mixing and defoaming in the above proportion that were respectively poured into the pores of the confocal dish and using silanized silicon wafers to cover the surface to ensure smooth. PDMS was cured in a drying oven at 65  $^{\circ}\text{C}$  overnight (12–24 h) and getting a 2 mm thick film. A PDMS of  $354.1 \pm 40.9$  kPa was obtained by using Sylgard 184 elastomer mixed with a matrix to curing agent ratio of 20:1. The theoretical value 350 kPa is used in this paper to calculate the contact stiffness. Using the spinning coating method, according to the adjustment of the

speed of the homogenizing machine to 4000 r/min, continue spinning coating for 50 s to form a PDMS film with a predetermined thickness of 20  $\mu\text{m}$ . After spin coating is completed, it is placed in a blast drying oven at 70  $^{\circ}\text{C}$  overnight for curing. Previous reports have shown that this curing time and temperature are sufficient for PDMS to fully cure, thus keeping the mechanical properties of PDMS unchanged during our experiments<sup>52</sup>.

### Micropattern of extracellular matrix proteins

Square patterns 324, 529, 1024, 2025, 4225 and 10,000  $\mu\text{m}^2$  were designed using Auto CAD software, and micropattern mold was prepared by the company. Pour the prepared Sylgard 184 elastomer into the mold wrapped in tin foil and heat it with a heating plate at 80  $^{\circ}\text{C}$  for 120 min. After cooling,

cut the PDMS seal. The prepared PDMS and stamp were ultrasounded in 75% alcohol for 15 minutes using a plasma cleaner and replaced with PBS. The seal and the prepared PDMS are processed for more than 15 minutes using a UV cleaning machine. The stamps were washed in sterile PBS that then the Hill ball was used to blow off the remaining. Using 10–50 µg/mL fibronectin (FN) coated with stamps and place on a super clean table for 1 h. Place the ozone-treated PDMS film in the 6-well plate that covered the side with FN stamp when pull out the stamp vertically to ensure the integrity of the pattern. Using 1% Pluronic reagent, soak for 5–10 min so that the cells only grow on the pattern. The Pluronic reagent was washed three times in PBS liquid to inoculate the cells.

### Cell culture

Human MSCs, HeLa cells, MDCK cells and MEFs were cultured in Dulbecco's modified eagle medium (DMEM) (containing with 4.5 g L<sup>-1</sup> glucose, l-glutamine, and sodium pyruvate) supplemented with 10% fetal bovine serum (FBS; Life Technologies, CA, USA), 100 IU mg<sup>-1</sup> penicillin–streptomycin (Life Technologies, CA, USA), and 1% (v/v) nonessential amino acids (NEAA; Life Technologies, CA, USA) at 37°C and 5% CO<sub>2</sub>.

### Immunocytochemical staining

Cells were fixed with 4% paraformaldehyde for 30 min at room temperature. After cell membrane was broken using 0.2% Triton X-100 for 10 min at room temperature, samples were blocked with 5% bovine serum albumin for 2 h. The samples were then incubated with primary antibodies against β1 integrin (1:200; Abcam), YAP (1:200; Abnova), RUNX2 (1:200; Abcam), Collagen I (1:200; Abcam) at 4 °C overnight. The samples were then incubated with secondary antibodies with fluorescence FITC (1:500; Abcam), TRITC (1:500; Abcam) or cy5 (1:200; Abcam) for 2 h at 37 °C. After staining cell nuclei and F-actin by DAPI (1:1000; Sigma) and phalloidin respectively samples were viewed under a Leica SP8 confocal microscopy system. Quantification of the immunofluorescence signal was performed by ImageJ software.

### Statistics and reproducibility

The data analysis was processed by one-way analysis of variance using Excel and SPSS. Data were presented as mean ± standard error of mean (S.E.M.), and boxplot format data were presented as median ± min/max, as indicated in the corresponding figure legends. Sample size (n) for each statistical analysis was presented in the corresponding figure legends. Statistical significance was determined by the two-tailed Student's t-test and one-way ANOVA with Tukey's correction, as indicated in the corresponding figure legends. Tukey's post-hoc test was used for multiple post-hoc comparisons to determine the significance between the groups after one-way analysis of variance (ANOVA). *P* < 0.05 was considered statistically significant. Statistical analysis was carried out using commercial software IBM SPSS Statistics 22.

### Calculation of contact stiffness

In cases where the ECM is far thicker than a cell (> 10-fold), CS was calculated with  $S = C_0 E^* \sqrt{A}$ , where  $C_0$  is a constant and taken as  $2/\sqrt{\pi}$ ;  $E^* = E/(1 - \nu^2)$  is the plane-strain modulus (which defines ECM stiffness),  $E^*$  is measured with indentation tests (Optics11, PIUMA) and tip with radius of 10 µm is used.; and  $A$  is the cell-ECM contact area measured in experiments.

When the ECM thickness must be considered (*i.e.*, ECM thickness is on the same order as the dimensions of the cell), CS was calculated with  $S = E^* \sqrt{A} \Pi(\sqrt{A}/t)$ , where  $\Pi$  is a dimensionless function as determined by Cao et al.<sup>29</sup> and  $t$  is the ECM thickness. For this situation, the steps for calculating CS are as follows:

- (1) Use formula  $E^* = E/(1 - \nu^2)$  to calculate the plane strain modulus  $E^*$ , where  $E$  and  $\nu$  are the elastic Modulus and Poisson's ratio of ECM.
- (2) Measure the size of the cell spreading area (contact area  $A$  between cells and the ECM).

(3) Calculate the shape factor  $C_0$ . Wang et al.<sup>53</sup> developed a theoretical model for accurately determining the contact stiffness of multi-indenter contact interface, which can calculate the contact stiffness of various contact interfaces with complex and irregular structures.

(4) Calculate the infinite stiffness parameter  $\Pi$ . Cao et al.<sup>29</sup> provided a calculation formula, as shown in

$$P = \frac{2E}{1 - \nu^2} ah \left( \frac{a}{t}, \nu \right) \quad (1)$$

and the dimension-less function is normalized first by using

$$f = 1.03e^{(-\frac{a}{t})} + \frac{\pi}{2} \frac{(1 - \nu^2)}{1 - 2\nu} \frac{a}{t} \left[ 1 - e^{(-\frac{a}{t})} \right] \quad (2)$$

The size of  $a/t$  corresponding to different  $\Pi$  can be obtained by searching the chart provided by Cao et al., where

$$a/t = \sqrt{A}/\sqrt{\pi t} \quad (3)$$

To explore the effect of non-adjacent layer on cell behavior, a two-layer hydrogel resting on the stiff substrate has been used. To calculate the contact stiffness of this two-layer ECM, for measured contact area  $A$ , layer thickness  $t_1, t_2$ , elastic moduli  $E_1, E_2$ , Poisson ratio  $\nu_1$  and  $\nu_2$ , finite element simulations as described below were performed to determine the contact stiffness. In our experiment, due to the thickness of the two layers of ECM, a simplified model proposed by Gao et al.<sup>28</sup> can be used to consider the double-layer ECM as a material with a thin film on substrate. the calculation formula for contact stiffness is

$$\frac{dP}{dh} = \frac{4\sqrt{A}}{\sqrt{\pi}} \frac{[\mu_1 I_0 + \mu_2 (1 - I_0)]}{1 - [\nu_1 I_1 + \nu_2 (1 - I_1)]} \quad (4)$$

Where  $\mu_1 = E_1/[2(1 + \nu_1)]$ ,  $\mu_2 = E_2/[2(1 + \nu_2)]$  and  $\xi = \sqrt{\pi t_1}/\sqrt{A}$

$$I_1 = \frac{2}{\pi} \arctan \xi + \frac{\xi}{\pi} \ln \frac{1 + \xi^2}{\xi^2} \quad (5)$$

$$I_0 = \frac{2}{\pi} \arctan \xi + \frac{1}{2\pi(1 - \nu)} \left[ (1 - 2\nu)\xi \ln \frac{1 + \xi^2}{\xi^2} - \frac{\xi}{1 + \xi^2} \right] \quad (6)$$

In cases where the ECM is far thicker than a cell (>10-fold), CS can be expressed as  $S = C_0 E^* \sqrt{A}$ <sup>29</sup>, where  $C_0$  is a constant;  $E^*$  is the plane-strain modulus (which defines ECM stiffness); and  $A$  is the contact area<sup>30</sup>.

### Finite element simulations

To determine the contact stiffness and the effect of contact geometry on the contact stiffness, the finite element analyses (FEA) was performed using Abaqus/standard (Abaqus 6.14, Dassault Systèmes®). In the simulation, a three-dimensional finite element model has been built, for a given contact area, we imposed normal displacement in the contact area and calculated the reaction force of the two-layer ECM, based on which the contact stiffness was calculated. We used a uniform mesh grid (element size 0.1 mm) in the contact area, and gradient grid in other areas (element size from 0.1 mm to 1.0 mm). The hybrid element C3D10MH (10-node modified tetrahedron element with hourglass control) was used in the whole model.

To study the effect of contact geometry on the contact stiffness, we changed the ratio of  $a/b$  of the elliptical contact region (as shown in Supplementary Fig. S9), where  $a$  and  $b$  are the semi-major and semi-minor axis, respectively. The ECM was assumed to be nearly incompressible (Poisson's ratio is taken as 0.49995) and elastic modulus was taken as 10 kPa. The displacement boundary was set in the contact area with lower boundary

fixed. From the given displacement and calculated reaction force, the contact stiffness was calculated.

### CS-based motor clutch model

Following the classical motor clutch framework<sup>54</sup>, intracellular force generated from the myosin can be transmitted from the F-actin bundles to the ECMs through the adhesion dynamics, and the molecular clutches within cell adhesions randomly bind between the F-actin and the ECM, thereby inducing ECM deformation. The mean-field theory is applied to approximate the stochastic processes of clutches. In our proposed CS-based motor clutch model, the relationship between cell adhesion force and substrate deformation is governed by CS, *i.e.*,  $S = E^* \sqrt{A} \Pi(\sqrt{A}/t)$ , which integrates substrate modulus, thickness, and cell-ECM contact area into one quantity; as the contact area changes with the cell spreading, the CS would vary during the iteration, which in turn affects the force equilibrium as well as the cell spreading area. A detailed description of the model formulation, theoretical derivations, and implementation details can be found in SI Note 1. All theoretical calculations of the CS-based motor clutch model were performed using MATLAB.

### Reporting summary

Further information on research design is available in the Nature Portfolio Reporting Summary linked to this article.

### Data availability

All data reported in this paper will be shared by the lead contact upon request. The source data supporting the graphs have been deposited in Figshare under the accession at <https://doi.org/10.6084/m9.figshare.30030433>. Any other relevant data that support the findings of this study are available from the corresponding author upon reasonable request.

### Code availability

All code reported in this paper will be shared by the lead contact upon request. The code of contact stiffness-based motor clutch model of this study is openly available in GitHub repository at <https://github.com/gongze/Contact-stiffness-model>. Any other relevant code that supports the findings of this study is available from the corresponding author upon reasonable request.

Received: 22 July 2025; Accepted: 15 October 2025;

Published online: 25 November 2025

### References

- Discher et al. Tissue cells feel and respond to the stiffness of their substrate. *Science* **310**, 1139–1143 (2005).
- Vogel, V. & Sheetz, M. Local force and geometry sensing regulate cell functions. *Nat. Rev. Mol. Cell Biol.* **7**, 265–275 (2006).
- Atcha, H., Choi, Y., Chaudhuri, O. & Engler, A. Getting physical: material mechanics is an intrinsic cell cue. *Cell Stem Cell* **30**, 750–765 (2023).
- Swift, J. et al. Nuclear lamin-a scales with tissue stiffness and enhances matrix-directed differentiation. *Science* **341**, 1240104 (2013).
- Wei, S. et al. Matrix stiffness drives epithelial-mesenchymal transition and tumour metastasis through a TWIST1-G3BP2 mechanotransduction pathway. *Nat. Cell Biol.* **17**, 678–688 (2015).
- Engler, A., Sen, S., Sweeney, H. & Discher, D. Matrix elasticity directs stem cell lineage specification. *Cell* **126**, 677–689 (2006).
- Sen, S., Engler, A. & Discher, D. Matrix strains induced by cells: computing how far cells can feel. *Cell. Mol. Bioeng.* **2**, 39–48 (2009).
- Buxboim, A., Rajagopal, K., Brown, A. & Discher, D. How deeply cells feel: methods for thin gels. *J. Phys. Condens. Matter: Inst. Phys. J.* **22**, 194116 (2010).
- Lin, Y. C. et al. Mechanosensing of substrate thickness. *Phys. Rev E Stat. Nonlin. Soft. Matter Phys.* **82**, 041918 (2011).
- Dupont, S. et al. Role of YAP/TAZ in mechanotransduction. *Nature* **474**, 179–183 (2011).
- Nam, S., Gupta, V. K., Lee, H. P., Lee, J. Y. & Chaudhuri, O. Cell cycle progression in confining microenvironments is regulated by a growth-responsive TRPV4-PI3K/Akt-p27 Kip1 signaling axis. *Sci. Adv.* **5**, eaaw6171 (2019).
- Sunyer, R. et al. Collective cell durotaxis emerges from long-range intercellular force transmission. *Science* **353**, 1157–1161 (2016).
- Barriga, E., Franze, K., Charras, G. & Mayor, R. Tissue stiffening coordinates morphogenesis by triggering collective cell migration in vivo. *Nature* **554**, 523–527 (2018).
- Cai, P. et al. Bio-inspired mechanotactic hybrids for orchestrating traction-mediated epithelial migration. *Adv. Mater.* **28**, 3102–3110 (2016).
- Schrader, J. et al. Matrix stiffness modulates proliferation, chemotherapeutic response, and dormancy in hepatocellular carcinoma cells. *Hepatology* **53**, 1192–1205 (2011).
- Gonzalez-Molina, J. et al. Mechanical confinement and DDR1 signaling synergize to regulate collagen-induced apoptosis in rhabdomyosarcoma cells. *Adv. Sci.* **9**, e2202552 (2022).
- Gilbert, P. et al. Substrate elasticity regulates skeletal muscle stem cell self-renewal in culture. *Science* **329**, 1078–1081 (2010).
- Trappmann, B. et al. Extracellular-matrix tethering regulates stem-cell fate. *Nat. Mater.* **11**, 642–649 (2012).
- Vining, K. & Mooney, D. Mechanical forces direct stem cell behaviour in development and regeneration. *Nat. Rev. Mol. Cell Biol.* **18**, 728–742 (2017).
- Levental, K. et al. Matrix crosslinking forces tumor progression by enhancing integrin signaling. *Cell* **139**, 891–906 (2009).
- Tan, Y. et al. Matrix softness regulates plasticity of tumour-repopulating cells via H3K9 demethylation and Sox2 expression. *Nat. Commun.* **5**, 4619 (2014).
- Chan, C. & Odde, D. Traction dynamics of filopodia on compliant substrates. *Science* **322**, 1687–1691 (2008).
- Gong, Z. et al. Matching material and cellular timescales maximizes cell spreading on viscoelastic substrates. *Proc. Natl. Acad. Sci. USA* **115**, E2686–E2695 (2018).
- Elosegui-Artola, A., Trepats, X. & Roca-Cusachs, P. Control of mechanotransduction by molecular clutch dynamics. *Trends Cell Biol.* **28**, 356–367 (2018).
- Johnson, K. L. & Johnson, K. L. *Contact mechanics*. (Cambridge University Press, 1987).
- Scott, K., Fraley, S. & Rangamani, P. A spatial model of YAP/TAZ signaling reveals how stiffness, dimensionality, and shape contribute to emergent outcomes. *Proc. Natl. Acad. Sci. USA* **118**, <https://doi.org/10.1073/pnas.2021571118> (2021).
- Pharr, G., Oliver, W. C. & Brotzen, F. On the generality of the relationship among contact stiffness, contact area, and elastic modulus during indentation. *J. Mater. Res.* **7**, 613–617 (1992).
- Gao, H., Cheng-Hsin, C. & Jin, L. Elastic contact versus indentation modeling of multi-layered materials. *Int. J. Solids & Struct.* **29**, 2471–2492 (1992).
- Cao, Y., Ma, D. & Raabe, D. The use of flat punch indentation to determine the viscoelastic properties in the time and frequency domains of a soft layer bonded to a rigid substrate. *Acta Biomater.* **5**, 240–248 (2009).
- Sneddon, I. N. The relation between load and penetration in the axisymmetric Boussinesq problem for a punch of arbitrary profile. *Int. J. Eng. Sci.* **3**, 47–57 (1965).
- McBeath, Rowena, Pirone, DanaM., Nelson, CelesteM., Bhadriraju, Kiran & Chen, ChristopherS. Cell shape, cytoskeletal tension, and RhoA regulate stem cell lineage commitment. *Dev. Cell* **6**, 0 (2004).
- Hadden, W. et al. Stem cell migration and mechanotransduction on linear stiffness gradient hydrogels. *Proc. Natl Acad. Sci. USA* **114**, 5647–5652 (2017).

33. Choi, Yu. Suk et al. The alignment and fusion assembly of adipose-derived stem cells on mechanically patterned matrices. *Biomaterials* **33**, 0 (2012).
34. Porazinski, S. et al. YAP is essential for tissue tension to ensure vertebrate 3D body shape. *Nature* **521**, 217–221 (2015).
35. Kletzien, R. F., Perdue, J. F. & Springer, A. Cytochalasin A and B: inhibition of sugar uptake in cultured cells. *J. Biol. Chem.* **247**, 2964–2966 (1972).
36. Barriga, E. H., Franze, K., Charras, G. & Mayor, R. Tissue stiffening coordinates morphogenesis by triggering collective cell migration in vivo. *Nature* **554**, 523–527 (2018).
37. Feng, F., Feng, X., Zhang, D., Li, Q. & Yao, L. Matrix stiffness induces pericyte-fibroblast transition through YAP activation. *Front. Pharmacol.* **12**, 698275 (2021).
38. Gandin, A. et al. Broadly applicable hydrogel fabrication procedures guided by YAP/TAZ-activity reveal stiffness, adhesiveness, and nuclear projected area as checkpoints for mechanosensing. *Adv. Healthc. Mater.* **11**, e2102276 (2022).
39. Benjamin, G., Joachim P., S. & Alexander D., B. Environmental sensing through focal adhesions. *Nat. Rev. Mol. Cell. Biol.* **10**, <https://doi.org/10.1038/nrm2593> (2009).
40. Benjamin L. et al. Determinants of maximal force transmission in a motor-clutch model of cell traction in a compliant microenvironment. *Biophys. J.* **105**, <https://doi.org/10.1016/j.bpj.2013.06.027> (2013).
41. Ovijit, C. et al. Substrate stress relaxation regulates cell spreading. *Nat. Commun.* **6**, <https://doi.org/10.1038/ncomms7365> (2015).
42. Adebowale, K., Gong, Z., Hou, J.C. et al. Enhanced substrate stress relaxation promotes filopodia-mediated cell migration. *Nat. Mater.* **20**, 1290–1299 (2021).
43. Xue, R., Chen, Y., Gong, Z. & Jiang, H. Superposition of Substrate Deformation Fields Induced by Molecular Clutches Explains Cell Spatial Sensing of Ligands. *ACS Nano*. **18**, 21144–21155 (2024).
44. Yang, M. T., Fu, J., Wang, Y. K., Desai, R. A. & Chen, C. S. Assaying stem cell mechanobiology on microfabricated elastomeric substrates with geometrically modulated rigidity. *Nat. Protoc.* **6**, 187–213 (2011).
45. Li, C., Zheng, L. & Fan, Y. Biophysical cues involved in the stem cell niche for stemness maintenance. *Med. Nov. Technol. Dev.* **22**, 100301 (2024).
46. Ronaldson-Bouchard, K. et al. Advanced maturation of human cardiac tissue grown from pluripotent stem cells. *Nature* **556**, 239–243 (2018).
47. Karamanos, N. et al. A guide to the composition and functions of the extracellular matrix. *FEBS J.* **288**, 6850–6912 (2021).
48. Gao, H. & Wu, T.-W. A note on the elastic contact stiffness of a layered medium. *J. Mater. Res.* **8**, 3229–3232 (1993).
49. Panzetta, V., Fusco, S. & Netti, P. Cell mechanosensing is regulated by substrate strain energy rather than stiffness. *Proc. Natl. Acad. Sci. USA* **116**, 22004–22013 (2019).
50. Yang, F. Contact stiffness of initially stressed neo-Hookean solids. *J. Polym. Sci. Part B: Polym. Phys.* **42**, 2513–2521 (2004).
51. Tse, J. & Engler, A. Preparation of hydrogel substrates with tunable mechanical properties. *Curr. Protoc. Cell Biol.* Unit 10.16, <https://doi.org/10.1002/0471143030.cb1016s47> (2010).
52. Rachele N. et al. Development of polydimethylsiloxane substrates with tunable elastic modulus to study cell mechanobiology in muscle and nerve. *PLoS One* **7**, e51499 (2012).
53. Wang, Y. et al. Contact stiffness of the multi-indenter contact interface. *J. Mech. Phys. Solids* **188**, 100022–105096 (2024).
54. Chan, C. E. & Odde, D. J. Traction dynamics of filopodia on compliant substrates. *Science* **322**, 1687–1691 (2008).

## Acknowledgements

This study was supported by the National Natural Science Foundation of China (NSFC) (11972206, 12222201, 82273500, 11572179, 11432008, 12472323, 12202439), the National Key R&D Program of China (2017YFA0506500) and Fundamental Research Funds for the Central Universities (ZG140S1971). We thank Dennis E. Discher (University of Pennsylvania), Song Li (University of California, Los Angeles), Bin Chen (Zhejiang University), Jiliang Hu (Tsinghua University), and Bo Wang (Chinese Academy of Sciences) for discussions during the preparation of this paper.

## Author contributions

Y.P.C. suggested the CS-based model, J.D., Y.P.C., and Z.G. designed and supervised the experiments and models, P.Z., Y.Z., Y.X.J and L.G. performed the experiments, Z.Y.Z., R.H.X., and M.W.J. developed the finite element model and motor clutch model. Y.N.G. and J.L.C. helped with the data analysis and all the authors took part in the data analysis. J.D., Y.P.C., and Z.G. wrote the paper.

## Competing interests

The authors declare no competing interests.

## Additional information

**Supplementary information** The online version contains supplementary material available at <https://doi.org/10.1038/s42003-025-09058-9>.

**Correspondence** and requests for materials should be addressed to Ze Gong, Jing Du or Yanping Cao.

**Peer review information** This manuscript has been previously reviewed at another journal. The manuscript was considered suitable for publication without further review at Communications Biology.

**Reprints and permissions information** is available at <http://www.nature.com/reprints>

**Publisher's note** Springer Nature remains neutral with regard to jurisdictional claims in published maps and institutional affiliations.

**Open Access** This article is licensed under a Creative Commons Attribution-NonCommercial-NoDerivatives 4.0 International License, which permits any non-commercial use, sharing, distribution and reproduction in any medium or format, as long as you give appropriate credit to the original author(s) and the source, provide a link to the Creative Commons licence, and indicate if you modified the licensed material. You do not have permission under this licence to share adapted material derived from this article or parts of it. The images or other third party material in this article are included in the article's Creative Commons licence, unless indicated otherwise in a credit line to the material. If material is not included in the article's Creative Commons licence and your intended use is not permitted by statutory regulation or exceeds the permitted use, you will need to obtain permission directly from the copyright holder. To view a copy of this licence, visit <http://creativecommons.org/licenses/by-nc-nd/4.0/>.

© The Author(s) 2025